High-Speed GeSi Electroabsorption Modulator on the SOI Waveguide Platform

Dazeng Feng, Wei Qian, Hong Liang, Cheng-Chih Kung, Zhou Zhou, Zhi Li, Jacob S. Levy, Roshanak Shafiiha, Joan Fong, B. Jonathan Luff, and Mehdi Asghari

(Invited Paper)

***Abstract*—Following significant research and development work over the past few years, silicon photonics has become a promising candidate to provide low-power, low-cost, and high-speed photonic links for telecommunication, data communication, and interconnect applications. A high-speed optical modulator is one of the critical components for these links. In this paper, we report on our recent progress in the development of a GeSi electro-absorption (EA) modulator based on the Franz–Keldysh effect (FKE) integrated in a 3-μm silicon-on-insulator (SOI) platform. We first discuss the FKE in GeSi, and describe the EA modulator device design and fabrication. We then report on the performance of the fabricated device. Finally, we describe the monolithic integration of four modulators with a four channel wavelength division multiplexing (WDM) echelle grating to demonstrate a 112 Gbit/s (4 $\times$ 28 Gbit/s) WDM transmitter chip. This chip establishes silicon photonics as an enabling technology for low-power and low-cost data transmission applications.**

***Index Terms*—Optical modulation, gratings, integrated circuits, silicon on insulator technology, wavelength division multiplexing.**

I. Introduction

NETWORK bandwidth requirements have been increasing exponentially, putting pressure on operators to meet demand while keeping infrastructure and power costs to a minimum. Silicon photonics, due to its integration capability, proven manufacturing record and attractive price–volume curve, is increasingly being recognized as the most viable platform to meet this challenge. Significant research and development work over the past few years [1]–[5] has resulted in many silicon photonics building blocks such as high-speed photodetectors [6]–[11], modulators [12]–[29], and WDM filters [30]–[40]. Among these components, silicon-based modulators still have many challenges that need to be overcome in order to achieve low-power, broadband, and high-speed operation. Owing to the weak linear electrooptic effect of silicon, most demonstrated waveguide-based silicon modulators utilize the free carrier dispersion effect with a Mach–Zehnder interferometer (MZI) or a ring resonator. Silicon MZI modulators are usually a few millimeters long and consume tens to hundreds of milliwatts. The silicon ring modulator has low power consumption, but an operating wavelength sensitive to fabrication and temperature which may require active tuning or additional wavelength locking. An alternative CMOS compatible material system, GeSi possesses a strong electro-absorption (EA) effect. The EA effect is known as the Franz–Keldysh effect (FKE) in bulk semiconductors and the quantum-confined Stark effect (QCSE) in quantum-well (QW) structures and is an intrinsically ultrafast process suitable for high-speed modulation. Liu *et al*. [15] first demonstrated a GeSi FK modulator integrated on a submicron silicon waveguide. High speed Ge FK modulators that work around 1620 nm have also been demonstrated using submicron waveguides [24]. Submicron waveguides enable high-speed operation, but suffer from large polarization discrimination and high fiber coupling loss. In contrast, high-speed Ge photodetectors [10], GeSi EA modulators [27], [28], and high performance optical multiplexers [38]–[40] have recently been demonstrated on 3 μm high SOI waveguides. The larger waveguide core provides polarization independent performance and low fiber coupling loss. For single mode operation, a 3-μm high waveguide has a width of 2.6 μm for a rib slab thickness of 1.8 μm with a propagation loss of less than 0.1 dB/cm. The bend radius can be less than 100 μm for a multimode waveguide by decreasing the rib slab thickness to 0.3 μm.

In this paper, we will review recent progress in the development of a high speed GeSi EA modulator including GeSi material properties, device design, fabrication, and measured performance. We then discuss the successful development of a compact, low-loss and high-speed WDM transmitter chip through monolithic integration of four GeSi EA modulators with a four channel 400 GHz-channel spacing echelle grating. The demonstrated GeSi EA modulator has a compact active region of 0.8 μm $\times$ 50 μm and a working wavelength range of 1525–1560 nm. The measured insertion loss of the device at 1540 nm is 4.8 dB and the dc extinction ratio is 5.9 and 3.8 dB with swing voltages of 3.0 and 2.0 V, respectively. The device can operate at 38 GHz with a 3.0-V reverse bias and 34 GHz with a 2.0-V reverse bias, as determined by the 3-dB bandwidth. A clear eye-opening at a transmission rate of 28 Gbps demonstrates the capability of high-bit-rate large signal modulation. The echelle grating has a 2.5-dB optical loss and the demonstrated WDM transmitter chip has over 100 Gbit/s aggregate transmission bandwidth and an overall link power penalty of 12 dB

Manuscript received March 14, 2013; revised June 11, 2013 and July 9, 2013; accepted August 9, 2013. Date of publication September 23, 2013; date of current version September 27, 2013.

The authors are with the Kotura Inc., Monterey Park, CA 91754 USA (e-mail: dfeng@kotura.com; wqian@kotura.com; hliang@kotura.com; ckung@kotura.com; jzhou@kotura.com; zli@kotura.com; jlevy@kotura.com; rshafiiha@kotura.com; jfong@kotura.com; jluff@kotura.com; masghari@kotura.com).

Color versions of one or more of the figures in this paper are available online at http://ieeexplore.ieee.org.

Digital Object Identifier 10.1109/JSTQE.2013.2278881

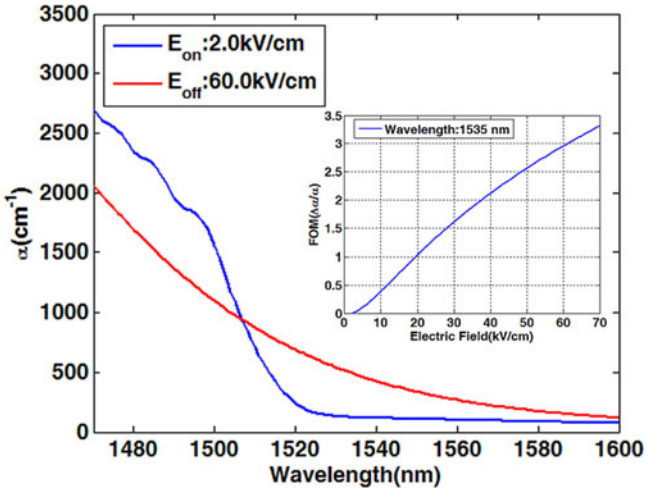

Fig. 1. Calculated $Ge_{1-x}Si_x$ $(x = 0.85\%)$ absorption coefficient as a function of wavelength for different electric fields. Inset: calculated FOM $(\Delta\alpha/\alpha_{\rm on})$ as a function of electric field.

which includes the total transmitter insertion loss, modulator extinction ratio penalty and modulation optical power loss.

II. Franz–Keldysh Effect in GeSi Material

The Franz–Keldysh effect (FKE) [42], [43] describes the electrooptic response in a bulk semiconductor. An applied electric field tilts the band edge, enhancing the absorption coefficient in the weak absorption region. A generalized FK theory can be used to calculate the absorption coefficient α [44]. We model the effect in the $Ge_{1-x}Si_x$ material system by linearly interpolating the intrinsic properties of Ge and Si. This approximation is valid when the Si composition x is less than few percent. The detailed description and values of the parameters for $Ge_{1-x}Si_x$ material can be found in [44]. The bandgap also depends on the material strain. When $Ge_{1-x}Si_x$ is grown on silicon, strain is introduced as a result of the coefficient of thermal expansion (CTE) mismatch between Si and $Ge_{1-x}Si_x$ and the temperature difference between growth temperature and room temperature. The in-plane strain is about 0.2% when the $Ge_{1-x}Si_x$ film is grown at around 700 °C. Fig. 1 shows the calculated absorption coefficient spectra for $Ge_{1-x}Si_x$ with a silicon composition of 0.85%. The details on the simulation method can be found in [14], [44], [46]. One of the basic figure of merit (FOM) for an EA modulator is $\Delta\alpha/\alpha_{\rm on}$ as it measures the ratio between the extinction ratio and the insertion loss, where $\alpha_{\rm on}$ is the on-state absorption coefficient (low electrical field), and $\Delta\alpha = \alpha_{\rm off} - \alpha_{\rm on}$ is the absorption coefficient difference between OFF state (high electrical field) and ON state. The inset in Fig. 1 shows the calculated $\Delta\alpha/\alpha_{\rm on}$ as a function of electric field. The theoretical $\Delta\alpha/\alpha_{\rm on}$ is close to 3.0 with an applied electric field of 60 kV/cm. Therefore, using this material composition, an EA modulator can have an insertion loss of 3 dB and an extinction ratio of 9.0 dB with an electric field of 60 kV/cm. However, the waveguide-based EA modulator suffers from losses other than bulk absorption. We must also consider the optical transition loss between the GeSi waveguide and the SOI waveguide,

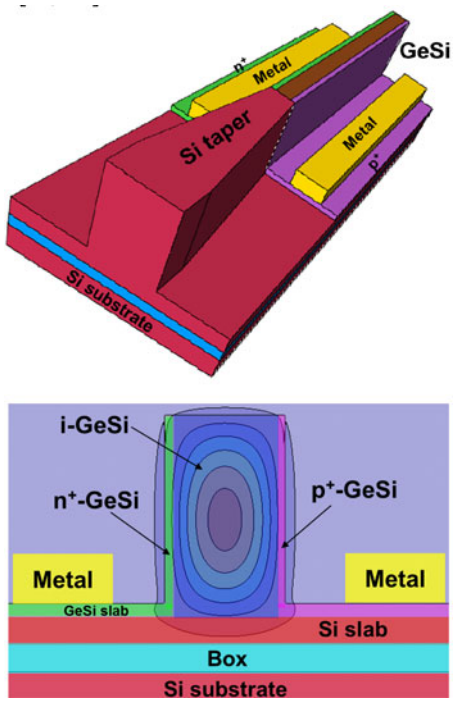

Fig. 2. Schematic and cross-sectional views of a GeSi FK modulator integrated with a 3-μm SOI waveguide.

free-carrier loss in the doped waveguide region and scattering loss from sidewall roughness. Additionally, a nonuniform electric field distribution will reduce field overlap with the optical mode, and consequently, will reduce $\Delta\alpha$. Therefore, the overall $\Delta\alpha/\alpha_{\rm on}$ of a waveguide-based EA modulator will be smaller compared to the results shown in Fig. 1 which only includes the material effect.

III. GeSi Modulator Design and Fabrication

The design of a high-speed FK modulator on the 3-μm waveguide platform provides a significant challenge due to the large waveguide core size. A possible solution is a vertical p-i-n junction, with a GeSi waveguide grown over the Si waveguide so that light evanescently couples to the GeSi region. However, the coupling length between the large cross-sectional waveguide and the GeSi waveguide in this configuration will be much longer than for submicron SOI devices. The excessive length will result in a large *RC* time delay, and thus, will limit the speed of the modulator. Instead of growing GeSi on top of the Si waveguide, we could butt-couple a vertical p-i-n junction GeSi to a large cross-sectional SOI waveguide. Although the device can be much shorter than an evanescently coupled device, the intrinsic GeSi region must be thick enough to match the SOI waveguide thickness, and thus, the electric field strength is limited. So, larger waveguides result in high capacitances or a weak electric field that limits the operation speed or increases the power consumption. To overcome these challenges, we have proposed and demonstrated a novel Ge/GeSi horizontally oriented p-i-n structure [10], [27]. The FK modulator and a cross section of the active p-i-n diode region are schematically shown in Fig. 2.

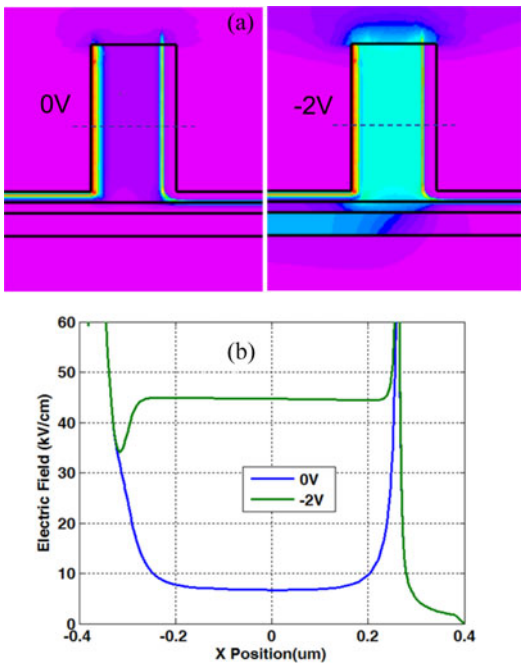

Fig. 3. (a) Simulated electric field in the p-i-n region at 0 V and -2 V bias. (b) Calculated electric field distribution along the dash line in (a).

The silicon waveguide width is reduced to match the GeSi waveguide width by a 50-μm long linear Si taper. As light propagates from the ridge SOI waveguide to the FK modulator region, it is butt-coupled to the active GeSi region. This butt-coupled configuration allows a good overlap between the SOI waveguide mode and the GeSi waveguide mode, and thus, makes a very short active length possible. The amount of absorption depends on the applied voltage across the p-i-n junction. This horizontal p-i-n configuration enables a very narrow intrinsic GeSi region, hence, reducing the voltage swing required to achieve a large electric field and high extinction ratio. The principal contributors to the insertion loss of the modulator are the GeSi material absorption loss and the mode mismatch loss between the silicon waveguide and the GeSi waveguide. The free-carriers caused loss in the sidewall doping region is small as the doping region has small overlap with optical mode and the device is only 50-μm long. The transition loss is calculated using the beam propagation method (BPM). The total transition loss is less than 0.5 dB when the silicon slab and GeSi slab are less than 0.3-μm thick for a 0.8-μm wide GeSi waveguide. Fig. 3 shows the simulated electric field distribution across the p-i-n junction at 0 and -2 V bias. The simulation shows a uniform electric field across the GeSi waveguide resulting in a good overlap with the optical mode. The electric field at 0 V bias is about 6 kV/cm due to the built-in voltage of the p-i-n diode of 0.35 V. With a reverse bias of 2 V, the electric field reaches 45 kV/cm. The EA modulator performance can be studied and simulated by considering the GeSi FK material effect and the electric field, free-carrier, and optical mode distributions. The details of the full simulation will be presented elsewhere.

We fabricate the modulator on six inch SOI wafers with a 0.4-μm thick buried oxide (BOX) and a 3-μm thick silicon epitaxial layer. We form a recess region by etching the silicon to 0.3-μm residual thickness above the BOX layer. We selectively grow a 100-nm thick GeSi buffer layer at 400 °C, followed by 4-μm thick GeSi growth at 670 °C inside the silicon recess region with a targeted Si composition of 0.85%. The GeSi film is intentionally over grown then thinned down and planarized with a chemical–mechanical polishing (CMP) step. The final GeSi thickness is 2.7 μm after CMP. We then anneal the wafers to reduce the threading dislocation density in the GeSi film. The silicon ridge waveguides, GeSi waveguides, and the silicon horizontal tapers are formed by the same etching step. As the etching rate of GeSi is greater than that of silicon, we perform a second etch of the silicon region to form a silicon ridge waveguide with a 0.3-μm thick slab and a GeSi ridge waveguide with a 0.3-μm thick slab. We do a sidewall implant of boron and phosphorus to form a horizontal p-i-n junction. The doping depths of phosphorus and boron are around 0.1 μm and 0.2 μm, respectively, estimated by the spreading resistance profiling (SRP) analysis. The surrounding slabs are doped to form p-type and n-type ohmic contacts. After rapid thermal annealing (RTA) dopant activation, we deposit a Ti/Al metal stack and pattern it to form p-type and n-type contacts. Finally, oxide and nitride films are deposited as waveguide cladding and passivation layers. The metal is covered by passivation layer to prevent the metal oxidation. A cross-sectional SEM image of the final fabricated device is shown in Fig. 4.

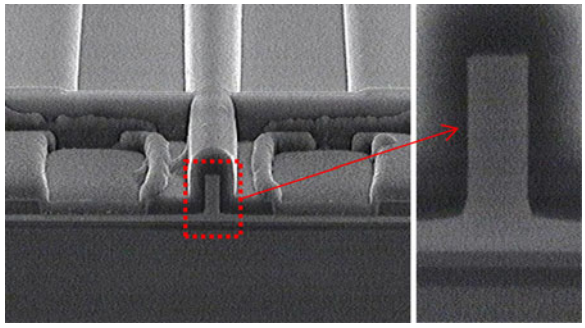

Fig. 4. Top view and cross-sectional view SEM images of the fabricated EA modulator.

In order to extract GeSi material properties, we fabricated an EA modulator with a very wide GeSi waveguide width of 2 μm. By using a wider waveguide device, we reduce the effect of sidewall doping and the device behavior is dominated by material effect. Fig. 5 shows the measured insertion loss and the extinction ratio of the device. The measured $\Delta\alpha/\alpha_{\rm on}$ reaches a maximum at wavelength of 1535 nm. We plot the extracted dependence of $\Delta\alpha/\alpha_{\rm on}$ on the electric field and the simulated results in Fig. 6. For a 60 kV/cm electric field, the extracted $\Delta\alpha/\alpha_{\rm on}$ reaches 2.6 which agrees well with the theoretical value given in Fig. 6. The remaining discrepancy between our measurement and theory results from the additional optical transition loss between the GeSi waveguide and the SOI waveguide, free-carrier loss, and propagation loss in the waveguide. So in a bulk material, the $\Delta\alpha/\alpha_{\rm on}$ should be larger than the results extracted from the 2-μm EA modulator.

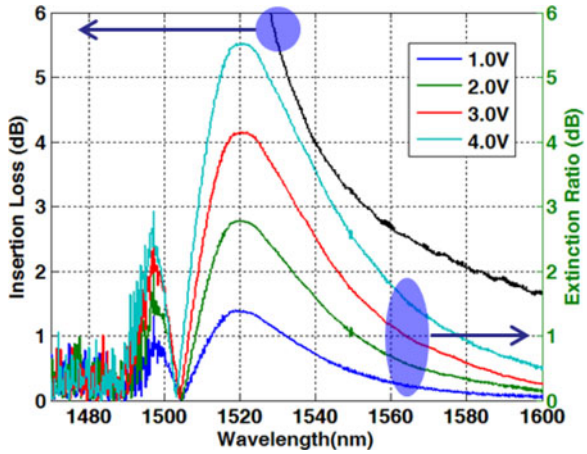

Fig. 5. Insertion loss and extinction ratio at different reverse biases for the EA modulator with a GeSi waveguide width of 2 μm.

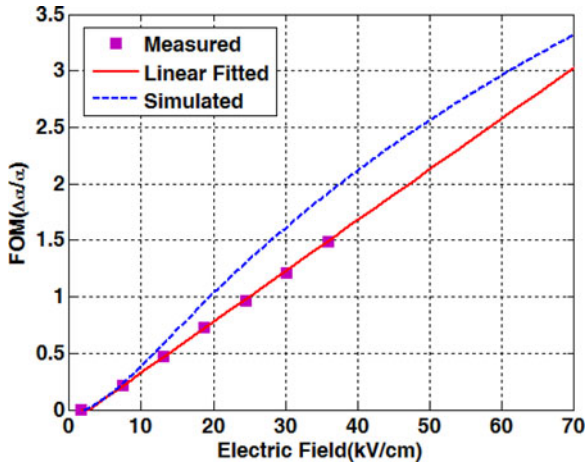

Fig. 6. Extracted FOM ($\Delta\alpha/\alpha_{\rm on}$) dependence on electric field based on the measured results of a 2-μm wide EA modulator.

IV. Performance of High-Speed GeSi EA Modulator

For a modulator with an active area of 0.8 μm $\times$ 50 μm, we measure the leakage currents at biases of -1.0 V, -2.0 V, and -3.0 V to be 1.2 μA, 5.7 μA, and 15.4 μA, respectively. In Fig. 7, we plot the full *I–V* characteristics of the fabricated FK modulator device. The dark current reported here is significantly reduced compared to previous modulator device [28] by optimization of the GeSi material growth and postannealing conditions, and by over etch of the Ti/Al to remove the metal residue. Therefore, the heating induced transmission spectra red shift caused by the dark current is negligible. To measure the devices, we couple the light from a tunable laser through a lensed fiber to the edge facet of the device. The light from the output waveguide was coupled to another lensed fiber which is then connected to a spectrum analyzer. In Fig. 8, we show the measured transmission spectra for different applied reverse bias voltage at room temperature. The measurements are normalized to a neighboring straight waveguide. Fig. 9 shows the extracted insertion loss and extinction ratios from 1470 to 1600 nm. At a wavelength of 1540 nm, the insertion loss is 4.8 dB, and the extinction ratio is 5.9 and 3.8 dB at 25 °C with 3 and 2 V reverse biases, respectively.

An attractive property of the EA modulator is its broad wavelength range operability. To quantify the operation bandwidth,

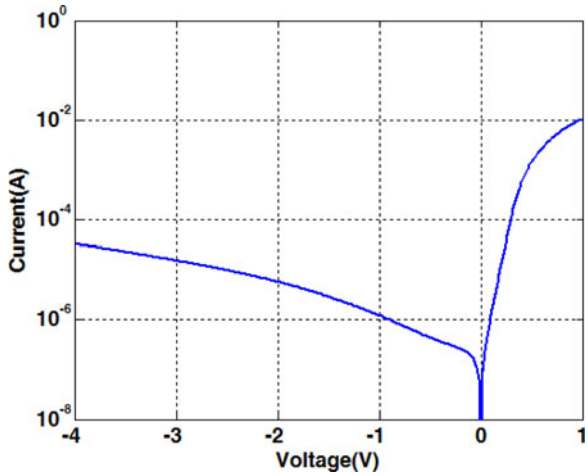

Fig. 7. Measured *I–V* characteristics of the fabricated GeSi modulator with an active area of 0.8 μm $\times$ 50 μm.

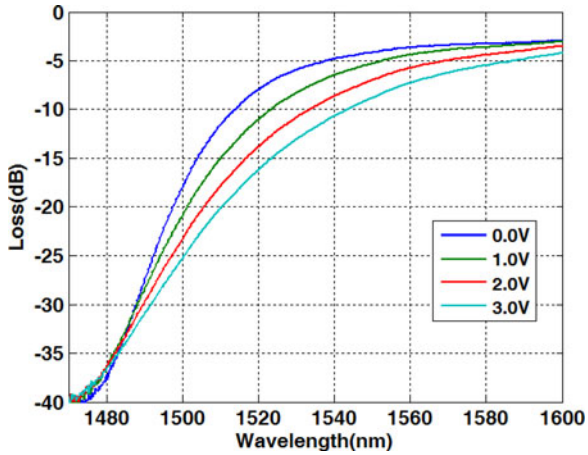

Fig. 8. Measured transmission spectra for different applied reverse voltages.

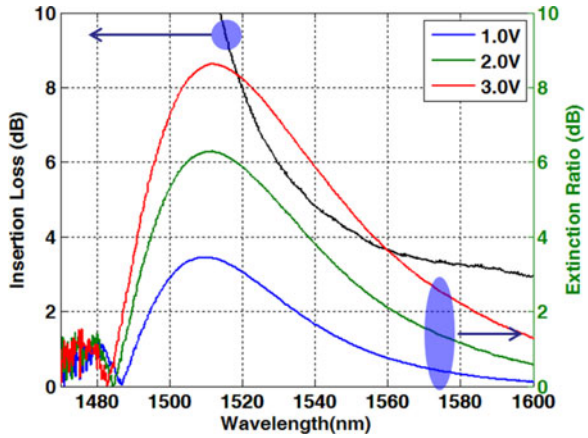

Fig. 9. Insertion loss and extinction ratio at different revise biases calculated based on the transmission spectra in Fig. 8.

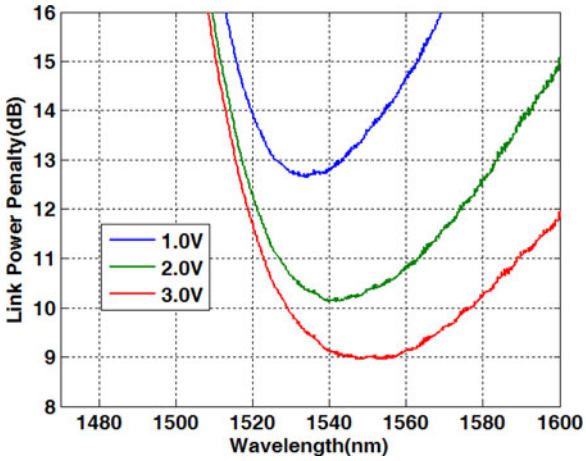

Fig. 10. Link power penalty of FK modulator for different applied reverse voltages.

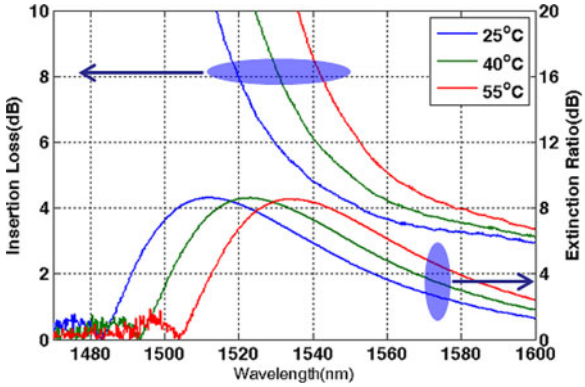

Fig. 11. Measured insertion loss and extinction ratio at different temperatures.

we define the link power penalty of a modulator [28], [47], [48] as OMA/$(2^{*}P_{\rm in}) = (P_{\rm out}(1) - P_{\rm out}(0))/(2P_{\rm in})$, where OMA $= P_{\rm out}(1) - P_{\rm out}(0)$ is the optical modulation amplitude, $P_{\rm in}$ is the input optical power to the modulator, and $P_{\rm out}(1)$ and $P_{\rm out}(0)$ are the high level and low level of the output optical powers after the modulator, respectively. Fig. 10 shows the link power penalty of the demonstrated EA modulator. The link power penalty of a modulator includes the insertion loss, modulation optical power loss, and limited extinction ratio penalties. The minimum link power penalty is 9.0 dB and the device has a 1dB optical bandwidth of over 40 nm with a 3-V driving voltage. At 2-V driving voltage, the minimum link power penalty is 10.2 dB and the 1-dB optical bandwidth is 40 nm. The temperature dependence of the transmission spectra of the GeSi FK modulator at different bias voltages is measured by using a thermal electric cooler (TEC) under the FK modulator chip. In Fig. 11, we show the measured insertion loss and extinction ratio for three temperature settings. The rate of the band edge shift is 0.76 nm/ °C [10], [28]. Consequently, the insertion loss and extinction ratio curves shift to longer wavelengths, but there is no performance degradation due to temperature change.

The high speed bandwidth of the EA modulator was measured by a 67-GHz lightwave component analyzer (LCA). We calibrate the RF system before measurements to factor out the

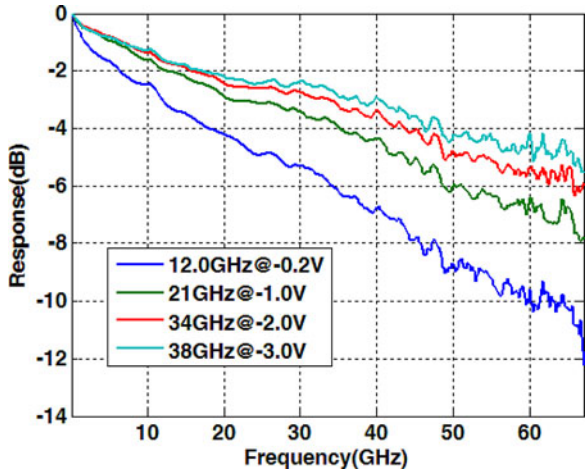

Fig. 12. Measured frequency response for the EA modulator based on FKE for different reverse biases.

effects of the cables, the bias-tee, and the photodetector response. Fig. 12 shows the measured frequency response of the EA modulator with various reverse bias voltages. The electrooptical bandwidths are 34 and 38 GHz at biases of -2 and -3 V, respectively. The FK effect has a response time on the subpicosecond scale [45], so the speed of an EA modulator based on the FK effect is limited by the *RC* time delay. The width of the intrinsic region of the p-i-n junction increases with higher reverse bias due to depletion. The larger depletion width yields a smaller capacitance so the modulator speed increases with higher reverse bias.

To demonstrate large signal high-speed modulation of the EA modulator, a pseudorandom binary sequence (PRBS) signal with a $(2^{31}–1)$ pattern length at a 28-Gbps transmission rate is set to swing from -1.5 to $+1.5$ V, and then, combined with a -1.5-V dc bias using a bias tee. The combined signal is then connected to the modulator through an electrical probe with 50-Ω termination. The eye-diagrams at 1530 nm, 1540 nm, 1550 nm, and 1560 nm wavelength are measured and shown in Fig. 13. Clear eye openings with dynamic extinction ratios of 6.3 dB, 5.4 dB, 4.5 dB, and 3.4 dB are, respectively, achieved with a 3.0-V swing voltage which are very close to the dc extinction ratio. Also, we measure the eye diagrams for different temperature at a fixed wavelength of 1560 nm. Fig. 14 shows the measured 28-Gbps optical eye diagrams at temperatures of 25 °C, 40 °C, 55 °C, and 70 °C. Clear eye openings with dynamic extinction ratios of 3.4 dB, 4.5 dB, 5.6 dB, and 6.7 dB, respectively, were achieved with a 3.0-V swing voltage. We also measured the rise and fall time of our EA modulator. Fig. 15 shows the measured rise time of 11 ps and fall time of 10.8 ps for the EA modulator. The measured rise and fall times of the driving signal from pulse pattern generator (PPG) are 10 and 9 ps, respectively. So the rise and fall times from the EA modulator only are 4.6 and 6.0 ps, respectively.

The S11 parameters of the EA modulator are measured in order to better understand the device's electrical properties and construct an equivalent circuit model to help in the modulator

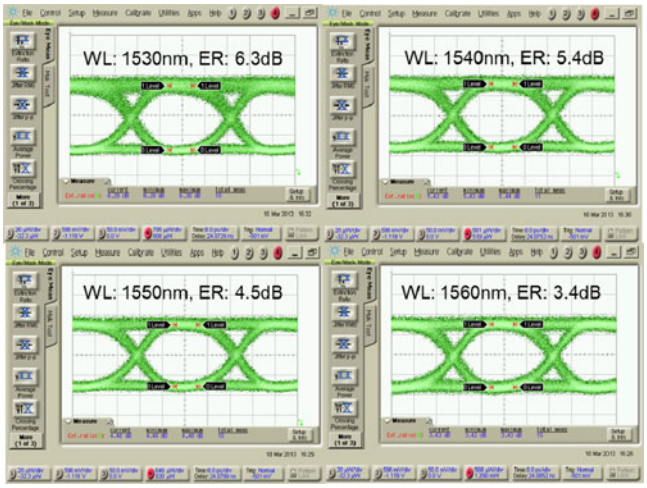

Fig. 13. Measured 28 Gbps eye diagrams at 25 °C at different wavelengths with a 3-V swing voltage.

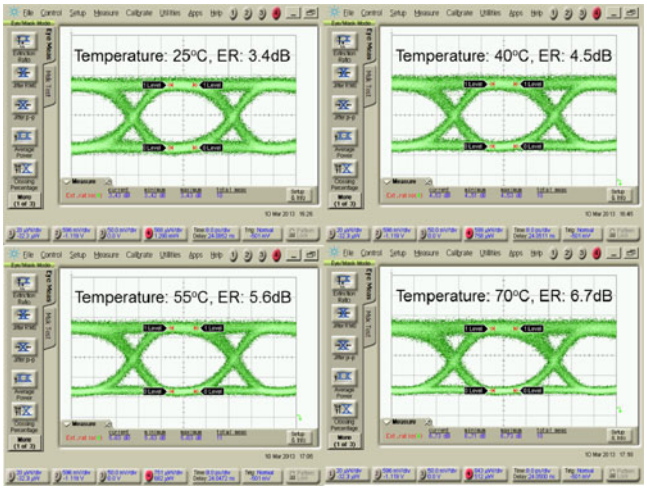

Fig. 14. Measured 28 Gbps eye diagrams at 1560 nm at different temperatures with a 3-V swing voltage.

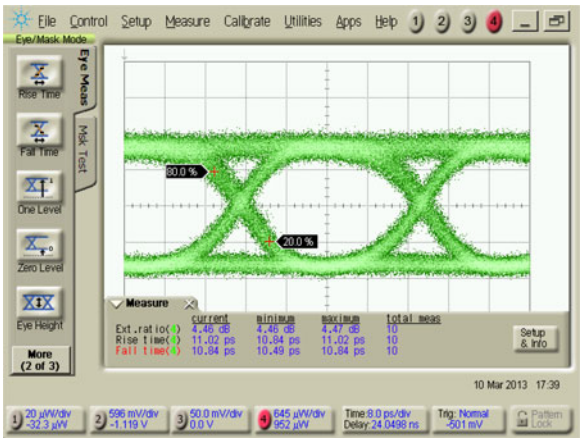

Fig. 15. Measured rise and fall time of the EA modulator with a 3-V swing voltage.

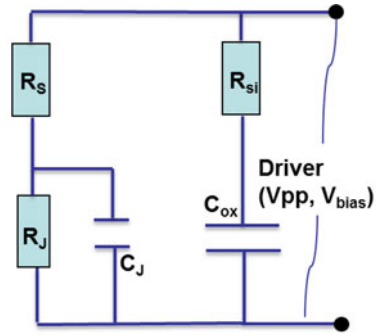

Fig. 16. Small signal circuit model of p-i-n EA modulator.

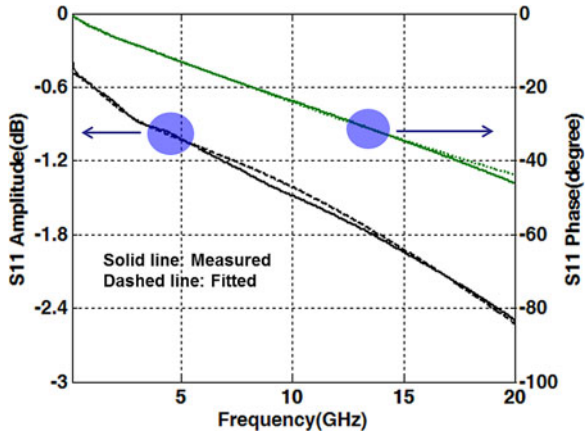

Fig. 17. Curve-fitting of the measured amplitude and phase of S11 at −1 V.

TABLE I
EXTRACTED RESISTANCE AND CAPACITANCE VALUES AT DIFFERENT BIASES

Symbol	0V	-1V	-2V	-3V
Rs (Ω)	40.3	34.7	33.1	32.4
C_J (fF)	109	78.0	69.6	65.2
R_J(kΩ)	1.36	1.77	1.73	1.67
R_{si}(kΩ)	0.89	1.55	1.76	1.90
C_{ox}(fF)	116	55.3	43.5	38.6

driver design. Fig. 16 shows the equivalent circuit for the modulator. R_S and C_J model the current path through the reverse-biased p-i-n junction, and R_J models the leakage current path. R_{Si} and C_{OX} model the current path through the silicon substrate and the buried oxide (BOX), respectively. The amplitude and the phase of the measured S11 parameters of the GeSi modulator are shown in Fig. 17. By fitting the S11 curves with the response of the equivalent circuit shown in Fig. 16 [41], the resistance and capacitance values are extracted and are summarized in Table I.

The junction capacitance of the EA modulator is estimated to be 65.2 fF at −3 V and 69.6 fF at −2 V, based on the measured S11. The average energy consumption per bit for the dynamic modulation is given by energy/bit $= 1/4 C_J \mathrm{V}_{\mathrm{pp}}^2$, where C_J is the junction capacitance, and V_{pp} is the swing voltage. The energy/bit for the demonstrated EA modulator with a swing voltage of 3.0 V and 2.0 V is approximately 147 fJ/bit and

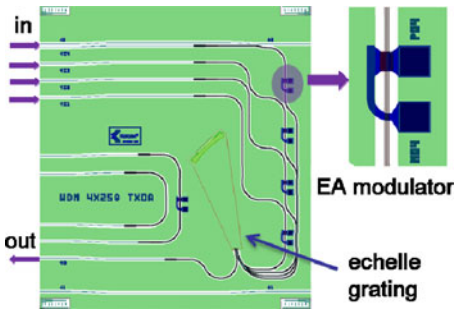

Fig. 18. Mask layout of 100 Gbps transmitter chip.

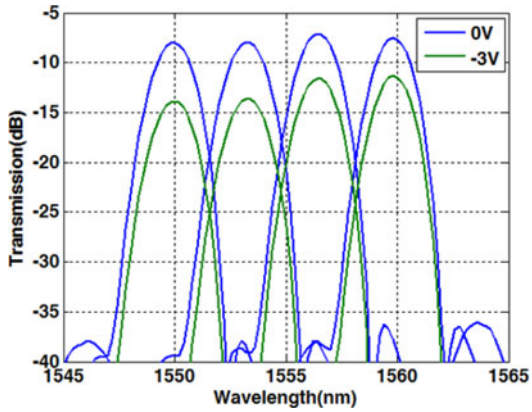

Fig. 19. Measured four channel spectra of the transmitter chip.

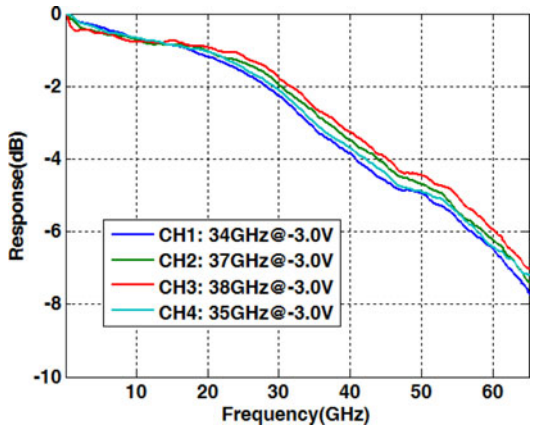

Fig. 20. Measured frequency response for the four channel WDM transmitter chip.

70 fJ/bit, respectively. The dynamic power consumption is about 4.1 and 2.0 mW with 3.0 and 2.0 V swing voltages, respectively for a 28-Gbps data transmission rate. The power consumption from the photogenerated currents is given by $1/2P_{\rm in}(R_{\rm on}V_{\rm on} + R_{\rm off}V_{\rm off})$. We measure the OFF state responsivity $R_{\rm off}$ of the EA modulator to be 0.8 A/W. The $V_{\rm on}$ is close to 0 V and $V_{\rm off}$ is close to the swing voltage $V_{\rm pp}$. The input optical power $P_{\rm in}$ to the modulator is limited to less than 6 mW for most applications. Therefore, including the photocurrent, the total power consumption is 11.3 and 6.8 mW with 3 and 2 V swing voltages, respectively, for a 28-Gbps modulation rate. With a swing voltage of 3.0 V, the modulator is suitable for a low power GeSi bipolar driver. Using the smaller 2-V swing, we can operate the demonstrated EA modulator with a CMOS driver.

V. 100 Gbit/s WDM Transmitter Chip

One of the key components in photonic links is a compact, low-cost, low-power WDM transmitter. Having demonstrated in the previous section a high-speed EA modulator based on the FKE, we now show that these devices can be successfully combined together to operate at a cumulative data rate higher than 100 Gbps by monolithically integrating four EA modulators and an echelle grating multiplexer with 400 GHz channel spacing on a single chip.

The mask layout of the WDM transmitter chip and a schematic view of the modulator are illustrated in Fig. 18. The device consists of a four channel echelle grating multiplexer and a four channel array of EA modulators. The incident and diffraction angles of the echelle grating are set to 28°, and 29°, respectively, to achieve sufficient angular dispersion. The grating diffraction order is selected as m = 29, so the loss caused by the diffraction envelop is less than 0.5 dB. The grating pitch, Λ, is 13.6 μm, which results in grating teeth with 12.0 μm wide reflecting facets. The wide reflection facets reduce the impact on grating performance due to teeth rounding. The grating line was adjusted from a Rowland circle mounting to minimize astigmatism by using a double-stigmatic point method [36]. The high speed EA modulators are located at the edge of the chip, so modulator drivers can be copackaged very close to the optical device enabling short wire bonds. Due to the demonstrated small parasitics, the EA modulator can be driven as a lumped element without the need for RF transmission lines. The WDM transmitter device is fabricated using standard CMOS compatible processes on 6-in SOI wafers with an epitaxial layer of 3-μm thick silicon. The fabricated four channel WDM transmitter chip has a footprint of 4 mm by 4.5 mm, and can be scaled down to much smaller footprint.

Fig. 19 shows the measured four channel spectra with 0 V and −3 V bias voltages applied to the EA modulators. We normalize the losses to a reference straight waveguide. We measure the average on-chip loss across the four channels of the transmitter chip to be 7.0 dB (2.5 dB from the echelle grating and 4.5 dB from the EA modulator). The average extinction ratio is about 4.5 dB. The link power penalty of the transmitter is about 12 dB which includes the transmitter insertion loss, modulation optical power loss and modulator limited extinction ratio penalties. The device has 400 GHz channel spacing and the echelle grating gives a 1-dB bandwidth of 120 GHz.

We measure 3-dB bandwidths greater than 34 GHz at a bias of −3 V for each modulator on the transmitter chip. In Fig. 20, we show the normalized frequency response as measured by a lightwave component analyzer. Given the small-signal 3-dB bandwidth measured at −3 V, we determine that devices are fast enough to transmit 28 Gbps optical signals. The 28 Gbps eye diagrams of four channels of the WDM transmitter are shown in Fig. 21 and for all four channels the eyes are open and clean. Combined, the four WDM channels, each capable

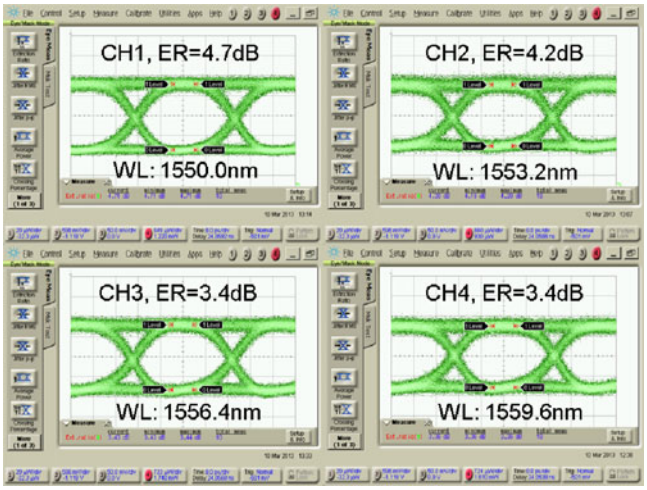

Fig. 21. Measured 28 Gbps eye diagrams for channels 1 to 4 with a 3-V swing voltage.

of transmitting a 28-Gbps signal, give a total bandwidth greater than 100 Gbit/s for our WDM transmitter.

VI. Conclusion

We have demonstrated a high speed GeSi EA modulator based on the FKE fully integrated with a 3-μm SOI waveguide with an operational wavelength in the C Band. The demonstrated modulator has a 3-dB bandwidth of 38 GHz, a broad operating wavelength range of 40 nm and a compact size of 0.8 μm $\times$ 50 μm. We have monolithically integrated the EA modulator with an echelle grating to demonstrate a four channel WDM transmitter chip. The WDM transmitter chip has a small footprint of 4 mm $\times$ 4.5 mm and an aggregate bandwidth of over 100 Gbit/s. By scaling our transmitter chip with more channels and operating at higher bitrates, we anticipate a potential WDM transmitter chip with a total bandwidth of over 1 Tbit/s. The small footprint and high performance of the reported device enables a low-cost, low-power WDM transmitter solution for high-speed data communication applications.

Acknowledgment

The authors would like to thank Dr. J. E. Cunningham, Dr. Y. Luo, Dr. X. Zheng, Dr. G. Li, Dr. K. Raj, and Dr. A. V. Krishnamoorthy from Oracle for helpful discussions and collaboration on early EA modulator work, and Dr. J. Liu from Dartmouth College for many helpful discussions on the GeSi EA modulator. The authors would like to acknowledge support from the DARPA UNIC program, funding the early EA modulator research.

References

[1] R. A. Soref, "The past, present and future of silicon photonics," *IEEE. J. Sel. Topics Quantum Electron.*, vol. 12, no. 6, pp. 1678–1687, Nov./Dec. 2006.

[2] L. C. Kimerling, D. Ahn, A. B. Apsel, M. Beals, D. Carothers, Y.-K. Chen, T. Conway, D. M. Gill, M. Grove, C.-Y. Hong, M. Lipson, J. Liu, J. Michel, D. Pan, S. S. Patel, A. T. Pomerene, M. Rasras, D. K. Sparacin, K.-Y. Tu, A. E. White, and C. W. Wong, "Electronic-photonic integrated circuits on the CMOS platform," *Proc. SPIE*, vol. 612502, pp. 6–15, 2006.

[3] B. Jalali and S. Fathpour, "Silicon photonics," *J. Lightw. Technol.*, vol. 24, no. 12, pp. 4600–4615, Dec. 2006.

[4] A. V. Krishnamoorthy, R. Ho, X. Zheng, H. Schwetman, J. Lexau, P. Koka, G. Li, I. Shubin, and J. E. Cunningham, "Computer systems based on silicon photonic interconnects," *Proc. IEEE*, vol. 97, no. 7, pp. 1337–1361, Jul. 2009.

[5] H. Liu, C. F. Lam, and C. Johnson, "Scaling optical interconnects in the datacenter networks: Opportunities and challenges for WDM," in *Proc. IEEE 18th Symp. High Perform. Interconnects*, 2010, pp. 113–116.

[6] J. Liu, D. Cannon, K. Wada, Y. Ishikawa, S. Jongthammanurak, D. Danielson, J. Michel, and L. C. Kimerling, "Tensile strained Ge *p-i-n* photodetectors on Si platform for C and L band telecommunications," *Appl. Phys. Lett.*, vol. 87, pp. 011110-1–011110-3, 2005.

[7] D. Ahn, C. Hong, J. Liu, W. Giziewicz, M. Beals, L. C. Kimerling, and J. Michel, "High performance, waveguide integrated Ge photodetectors," *Opt. Exp.*, vol. 15, pp. 3916–3921, 2007.

[8] L. Vivien, M. Rouviere, J. Fedeli, D. Marris-Morini, J. Damlencourt, J. Mangeney, P. Crozat, L. El Melhaoui, E. Cassan, X. Le Roux, D. Pascal, and S. Laval, "High speed and high responsivity germanium photodetector integrated in a Silicon-On-Insulator microwaveguide," *Opt. Exp.*, vol. 15, pp. 9843–9848, 2007.

[9] T. Yin, R. Cohen, M. Morse, G. Sarid, Y. Chetrit, D. Rubin, and M. Paniccia, "31GHz Ge n-i-p waveguide photodetectors on silicon-on-insulator substrate," *Opt. Exp.*, vol. 15, pp. 13965–13971, 2007.

[10] D. Feng, S. Liao, P. Dong, N.-N. Feng, H. Liang, D. Zheng, C.-C. Kung, J. Fong, R. Shafiiha, J. E. Cunningham, A. V. Krishnamoorthy, and M. Asghari, "High-speed Ge photodetector monolithically integrated with large cross-section silicon-on-insulator waveguide," *Appl. Phys. Lett.*, vol. 95, no. 26, pp. 261105-1–261105-3, 2009.

[11] J. Michel, J. Liu, and L. C. Kimerling, "High-performance Ge-on-Si photodetectors," *Nature Photon.*, vol. 4, pp. 527–534, 2010.

[12] Q. Xu, B. Schmidt, S. Pradhan, and M. Lipson, "Micrometer-scale silicon electro-optic modulator," *Nature*, vol. 435, pp. 325–327, 2005.

[13] A. Liu, L. Liao, D. Rubin, H. Nguyen, B. Ciftcioglu, Y. Chetrit, N. Izhaky, and M. Paniccia, "High-speed optical modulation based on carrier depletion in a silicon waveguide," *Opt. Exp.*, vol. 15, pp. 660–668, 2007.

[14] J. Liu, D. Pan, S. Jongthammanurak, K. Wada, L. C. Kimerling, and J. Michel, "Design of monolithically integrated GeSi electro-absorption modulators and photodetectors on a SOI platform," *Opt. Exp.*, vol. 15, pp. 623–628, 2007.

[15] J. Liu, M. Beals, A. Pomerene, S. Bernardis, R. Sun, J. Cheng, L. C. Kimerling, and J. Michel, "Waveguide-integrated, ultralow-energy GeSi electro-absorption modulators," *Nature Photon.*, vol. 2, pp. 433–437, 2008.

[16] P. Dong, S. Liao, D. Feng, H. Liang, D. Zheng, R. Shafiiha, C. C. Kung, W. Qian, G. Li, X. Zheng, A. V. Krishnamoorthy, and M. Asghari, "Low VPP, ultralow-energy, compact, high-speed silicon electro-optic modulator," *Opt. Exp.*, vol. 17, no. 25, pp. 22484–22490, 2009.

[17] N.-N. Feng, S. Liao, D. Feng, P. Dong, D. Zheng, H. Liang, R. Shafiiha, G. Li, J. E. Cunningham, A. V. Krishnamoorthy, and M. Asghari, "High speed carrier-depletion modulators with 1.4 V-cm VπL integrated on 0.25μm silicon-on-insulator waveguides," *Opt. Exp.*, vol. 18, no. 8, pp. 7994–7999, 2010.

[18] G. T. Reed, G. Mashanovich, F. Y. Gardes, and D. J. Thomson, "Silicon optical modulators," *Nature Photon.*, vol. 4, pp. 518–526, 2010.

[19] D. J. Thomson, F. Y. Gardes, Y. Hu, G. Mashanovich, M. Fournier, P. Grosse, J.-M. Fédéli, and G. T. Reed, "High contrast 40Gbit/s optical modulation in silicon," *Opt. Exp.*, vol. 19, no. 12, pp. 11507–11516, 2011.

[20] X. Zheng, D. Patil, J. Lexau, F. Liu, G. Li, H. Thacker, Y. Luo, I. Shubin, J. Li, J. Yao, P. Dong, D. Feng, M. Asghari, T. Pinguet, A. Mekis, P. Amberg, M. Dayringer, J. Gainsley, H. F. Moghadam, E. Alon, K. Raj, R. Ho, J. E. Cunningham, and A. V. Krishnamoorthy, "Ultra-efficient 10 Gb/s hybrid integrated silicon photonic transmitter and receiver," *Opt. Exp.*, vol. 19, pp. 5172–5186, 2011.

[21] G. Li, X. Zheng, J. Yao, H. Thacker, I. Shubin, Y. Luo, K. Raj, J. E. Cunningham, and A. V. Krishnamoorthy, "25 Gb/s 1 V-driving CMOS ring modulator with integrated thermal tuning," *Opt. Exp.*, vol. 19, pp. 20435–20443, 2011.

[22] M. R. Watts, D. C. Trotter, R. W. Young, and A. L. Lentine, "Ultralow power silicom microdisk modulators and switches," in *Proc. IEEE Conf. Group IV Photon.*, 2008, pp. 4–8.

[23] Y.-H. Kuo, Y. K. Lee, Y. Ge, S. Ren, J. E. Rothm, T. I. Kamins, D. A. B. Miller, and J. S. Harris, "Strong quantum-confined Stark effect in germanium quantum-well structures on silicon," *Nature*, vol. 437, p. 1334, 2005.

[24] A. E.-J. Lim, T.-Y. Liow, F. Qing, N. Duan, L. Ding, M. Yu, G.-Q. Lo, and D.-L. Kwong, "Novel evanescent coupled germanium electro-absorption modulator featuring monolithic integration with germanium p-i-n photodetector," *Opt. Exp.*, vol. 19, no. 6, pp. 5040–5046, 2011.

[25] P. Chaisakul, D. Marris-Morini, M. S. Rouifed, G. Isella, D. Chrastina, J. Frigerio, X. L. Roux, S. Edmond, J. Coudevylle, and L. Vivien, "23 GHz Ge/SiGe multiple quantum well electro-absorption modulator," *Opt. Exp.*, vol. 20, pp. 3219–3224, 2012.

[26] R. Shen, R. Yiwen, S. A. Claussen, R. K. Schaevitz, T. I. Kamins, J. S. Harris, and D. A. B. Miller, "Ge/SiGe quantum well waveguide modulator monolithically integrated with SOI waveguides," *IEEE Photon. Technol. Lett.*, vol. 24, no. 6, pp. 461–463, Mar. 2012.

[27] N. Feng, D. Feng, S. Liao, X. Wang, P. Dong, H. Liang, C-C. Kung, W. Qian, J. Fong, R. Shafiiha, Y. Luo, J. Cunningham, A. V. Krishnamoorthy, and M. Asghari, "30GHz Ge electro-absorption modulator integrated with 3μm silicon-on-insulator waveguide," *Opt. Exp.*, vol. 19, pp. 7062–7067, 2011.

[28] D. Feng, S. Liao, H. Liang, J. Fong, B. Bijlani, R. Shafiiha, B. J. Luff, Y. Luo, J. Cunningham, A. V. Krishnamoorthy, and M. Asghari, "High speed GeSi electro-absorption modulator at 1550 nm wavelength on SOI waveguide," *Opt. Exp.*, vol. 20, pp. 22224–22232, 2012.

[29] Y. Luo, X. Zheng, G. Li, I. Shubin, H. Thacker, J. Yao, H. Jin, D. Feng, J. Fong, C.-C. Kung, S. Liao, R. Shafiiha, M. Asghari, K. Raj, A. V. Krishnamoorthy, and J. Cunningham, "Strong Electro-Absorption in GeSi Epitaxy on Silicon-on-Insulator (SOI)," *Micromachines*, vol. 3, no. 2, pp. 345–363, 2012.

[30] P. D. Trinh, S. Yegnanarayanan, F. Coppinger, and B. Jalali, "Silicon-on-insulator (SOI) phased-array wavelength multi/demultiplexer with extremely low-polarization sensitivity," *IEEE Photon. Technol. Lett.*, vol. 9, no. 7, pp. 940–942, Jul. 1997.

[31] T. Fukazawa, F. Ohno, and T. Baba, "Very compact arrayed-waveguide grating demultiplexer using Si photonic wire waveguides," *Jpn. J. Appl. Phys.*, vol. 43, pp. L673–L675, 2004.

[32] W. Wang, Y. Tang, Y. Wang, H. Qu, Y. Wu, T. Li, J. Yang, Y. Wang, and M. Liu, "Etched-diffraction-grating-based planar waveguide demultiplexer on silicon-on-insulator," *Opt. Quantum Electron.*, vol. 36, pp. 559–566, 2004.

[33] J. Brouckaert, W. Bogaerts, P. Dumon, D. Van Thourhout, and R. Baets, "Planar concave grating demultiplexer fabricated on a nanophotonic silicon-on-insulator platform," *J. Lightw. Technol.*, vol. 25, no. 5, pp. 1269–1275, May 2007.

[34] J. Brouckaert, W. Bogaerts, S. Selvaraja, P. Dumon, R. Baets, and D. Van Thourhout, "Planar concave grating demultiplexer with high reflective Bragg reflector facets," *IEEE Photon. Technol. Lett.*, vol. 20, no. 4, pp. 309–311, Feb. 2008.

[35] F. Horst, W. M. J. Green, B. J. Offrein, and Y. A. Vlasov, "Silicon-on-insulator echelle grating WDM demultiplexers with two stigmatic points," *IEEE Photon. Technol. Lett.*, vol. 21, no. 23, pp. 1743–1745, Dec. 2009.

[36] R. Marz, *Integrated Optics Design and Modeling*. London, U.K.: Artech House, 1994.

[37] B. J. Luff, D. Feng, D. C. Lee, W. Qian, H. Liang, and M. Asghari, "Hybrid silicon photonics for low-cost high-bandwidth link applications," *Adv. Opt. Technol.*, vol. 2008, Article ID 245131, 6 pp., 2008. http://dx.doi.org/10.1155/2008/245131.

[38] D. Feng, W. Qian, H. Liang, C.-C. Kung, J. Fong, B. J. Luff, and M. Asghari, "Fabrication intensive echelle grating in silicon-on-insulator platform," *IEEE Photon. Technol. Lett.*, vol. 23, no. 5, p. 284, Mar. 2011.

[39] D. Feng, N-N. Feng, C-C. Kung, H. Liang, W. Qian, J. Fong, B. J. Luff, and M. Asghari, "Compact single-chip VMUX/DEMUX on the silicon-on-insulator platform," *Opt. Exp.*, vol. 19, pp. 6125–6130, 2011.

[40] D. Feng, W. Qian, H. Liang, N-N. Feng, S. Liao, C-C. Kung, J. Fong, Y. Liu, R. Shafiiha, D. C. Lee, B. J. Luff, and M. Asghari, "Terabit/s single chip WDM receiver on the SOI platform," in *Proc. IEEE 8th Int. Conf. Group IV Photon.*, 2011, pp. 320–322.

[41] G. Li, X. Zheng, J. Lexau, Y. Luo, H. Thacker, P. Dong, S. Liao, D. Feng, M. Asghari, J. Yao, J. Shi, P. Amberg, N. Pinckney, K. Raj, R. Ho, J. E. Cunningham, and A. V. Krishnamoorthy, "Ultralow-power, high-performance Si photonic transmitter," presented at the Optical Fiber Communication Conf. 2010, San Diego, CA, USA, 2010, paper no. OMI2.

[42] W. Franz, "Einflus eines elektrischen Feldes auf eine optische Absorptionskante," *Z. Naturforschung*, vol. 13a, pp. 484–489, 1958.

[43] L. V. Keldysh, "Behaviour of non-metallic crystals in strong electric fields," *J. Exptl. Theoret. Phys.*, vol. 33, pp. 994–1003, 1957.

[44] J. Liu, "GeSi photodetectors and electro-absorption modulators for Si electronic-photonic integrated circuits," Ph.D. thesis, Massachusetts Inst. Technol., Cambridge, MA, USA, 2007.

[45] J. F. Lampin, L. Desplanque, and F. Mollot, "Detection of picosecond electrical pulses using the intrinsic Franz-Keldysh effect," *Appl. Phys. Lett.*, vol. 78, pp. 4103–4105, 2001.

[46] X. Sun, "Ge-on-Si Light-Emitting Materials and Devices for Silicon Photonics," Ph.D. thesis, Massachusetts Inst. Technol., Cambridge, MA, USA, 2009.

[47] G. Li, X. Zheng, J. Yao, H. Thacker, I. Shubin, Y. Luo, K. Raj, J. E. Cunningham, and A. V. Krishnamoorthy, "25 Gb/s 1 V-driving CMOS ring modulator with integrated thermal tuning," *Opt. Exp.*, vol. 19, pp. 20435–20443, 2011.

[48] G. P. Agrawal, *Lightwave Technology*. New York, NY, USA: Wiley, 2005.

Dazeng Feng received the B.S. and Ph.D. degrees in optics from Fudan University, Shanghai, China, in 1986 and 1992, respectively, where from 1992 to 1995, he was a Faculty Member. From 1995 to 2000, he was a Research Scientist at Optiwave Corp. He is currently the Director of Photonics Technology at Kotura Inc, Monterey Park, CA, USA. He is currently working on silicon photonics He has more than 100 technical publications and holds more than 20 issued silicon photonics patents.

Wei Qian received the Ph.D. degree from the Institute of Microelectronics, Tsinghua University, Beijing, China, in 1998. He is currently a Principal Engineer at Kotura Inc., Monterey Park, CA, USA, a leading Si photonic company. His current research interests include Si photonic device integration, new technology, and process development.

Hong Liang received the B.Sc. degree in physical optics from Shandong University, Jinan, China, in 1984. She is currently a Principal Engineer and an R&D test Lab Manager at Kotura Inc., Monterey Park, CA, USA. Previously, she has served for The Institute of Physical and Chemical Research, Wako, Japan. She is currently responsible for the characterization of silicon photonics devices including optical modulator, photodetector, grating coupler, integrated WDM transmitter, and receiver.

Cheng-Chih Kung received the M.S. degree in electrical engineering from National Chiao Tung University, Hsinchu, Taiwan and the B.S. degree in electrical engineering from Tamkang University, Taipei, Taiwan. He joined Kotura Inc., Monterey Park, CA, USA, in 2001, and is responsible for process integration and thin film process development. Before Kotura Inc., he worked for United Microelectronics Corporation, Taiwan and was involved in process integration and customer engineering from 1992 to 2001. He has eight patents approved in the USA.

Zhou Zhou received the B.S. degree in electronic engineering from Southeast University, Nanjing, China, and the M.S. and Ph.D. degrees in photonics from the University of California at San Diego, San Diego, CA, USA. He is currently a Senior Development Engineer at Kotura Inc., Monterey Park, CA. His research interests include silicon photonic device physics, design, and testing.

Zhi Li received the B.S. degree in optical engineering from Zhejiang University, Hangzhou, China, in 2007, and the Ph.D. degree in electrical engineering from the University of Virginia, Charlottesville, VA, USA, in 2011. His graduate school research focused on high power high speed III–IV photodiode. He currently is a Senior Design Engineer at Kotura Inc., Monterey Park, CA, USA, focusing on Ge based photodetector on silicon platform.

Jacob S. Levy received the B.S. degree in electrical engineering from Duke University, Durham, NC, USA, in 2006 and the M.S. and Ph.D. degrees in electrical engineering from Cornell University, Ithaca, NY, USA, in 2010 and 2011, respectively. His graduate school research focused on nonlinear optical phenomena in integrated waveguides. He currently is a Senior Design Engineer at Kotura Inc., Monterey Park, CA, USA, focusing on active and passive optical devices in the silicon platform.

Roshanak Shafiiha received the Graduate degree from the University of Southern California, Los Angeles, CA, USA, in 2004 and the Ph.D. degree in electrical engineering. Then, she pursued two years of Postdoctoral Research followed by one year of independent research in biomedical imaging at the University of California, Irvine, CA. She received the DOD Multidisciplinary Postdoctoral Award in breast cancer research. Since January 2008, she has been with Kotura Inc., Monterey Park, CA, where she is a Senior Engineer in R&D group focusing on optical design and device characterization. She is also the Project Manager for some of Kotura's government funded projects.

Joan Fong received the Ph.D. degree in materials science/chemistry from the University of North Carolina at Chapel Hill, Chapel Hill, NC, USA, in 1995, and the B.S. and M.S. degrees in materials science from Tsinghua University, Beijing, China, in 1987 and 1989, respectively. She currently holds the position of the Fab. Manager at Kotura Inc., Monterey Park, CA, USA, also with a responsibility for dry etch process development. From 1995–2000, she was a Member of technical staff, Si etch division, at Applied Materials. She holds five U.S. patents in Si dry etch and optical device fabrication.

B. Jonathan Luff received the Ph.D. degree in physics from the University of Sussex, Brighton, U.K., and has more than 15 years of experience in silicon photonics research, design, and fabrication. He is currently the Director of product development at Kotura Inc., Monterey Park, CA, USA. He has published more than 40 technical articles and holds five issued patents.

Mehdi Asghari received the Ph.D. degree in optoelectronics from the University of Bath, Bath, U.K., the M.Sc. degree in optoelectronics and laser devices from the Heriot-Watt and St. Andrews Universities, U.K., and the B.A. degree in engineering from Cambridge University, U.K. He has more than 15 years of progressive engineering and management experience within the silicon photonics and optoelectronics industries. He is currently the CTO at Kotura Inc., Monterey Park, CA, USA. Prior to this, he served as a VP Research and Development of Bookham, Inc., San Jose, CA. He has authored or coauthored more than 100 publications and holds more than 20 patents within the fields of silicon photonics and optoelectronics.